University of Nebraska - Lincoln

DigitalCommons@University of Nebraska - Lincoln

2020

Origin of the multiphoton-regime harmonic-generation plateau structure

Jean Marcel Ngoko Djiokap

Anthony F. Starace

Origin of the multiphoton-regime harmonic-generation plateau structure

J. M. Ngoko Djiokap ●[*] and Anthony F. Starace[†]

Department of Physics and Astronomy, University of Nebraska, Lincoln, Nebraska 68588-0299, USA

A physical interpretation is provided for the formation of the multiphoton-regime plateau feature in the spectra of nonlinear and correlated process of high-order harmonic generation (HHG) of two-active-electron atoms interacting with an intense linearly polarized laser field [Phys. Rev. A **88**, 053412 (2013) for beryllium]. While in the strong-field tunneling regime the plateau feature is well known to be due to rescattering effects of the freed electron, its counterpart in the multiphoton regime is due to atomic resonance effects involving both singly excited states and doubly excited states. Here, we propose a strategy to uncover which kind of these states are responsible for this phenomenon. By studying the sensitivity of HHG to the initial state in helium, we show that this multiphoton-regime plateau structure mostly originates from singly excited states.

I. INTRODUCTION

The discovery of high-order harmonic generation (HHG) experimentally in the late 1980s was based on rare gases [1–7], which are multielectron systems. To produce short-wavelength harmonics of the fundamental of the driving laser field, a first group [5,7] used long-wavelength driving lasers (iodine-laser radiation at 1315 nm and Nd:YAG laser at 1064 nm); while a second group [1–4,6] used short-wavelength driving lasers in the range 266–307 nm. In the former case, HHG occurs in the low-frequency tunneling regime defined by a Keldysh parameter $\gamma = \sqrt{E_b/2U_p} < 1$, where E_b is the target binding energy and U_p is the electron ponderomotive energy. In this low-frequency tunneling regime, the three-step scenario [8–10] (i.e., ionization by tunneling, laser-driven electron motion away from and back to the target ion, and recombination of the electron with harmonic emission) has proved to be an invaluable guide for understanding and planning HHG experiments. In the latter case, HHG occurs in the multiphoton regime defined by $\gamma > 1$ where this simple-man's model [8–10] is no longer applicable. Although this simple-man's model for multielectron targets is usually thought in terms of single-active-electron approximation, multielectron effects must manifest themselves in the HHG produced in both the tunneling regime and the multiphoton regime.

In the tunneling regime, the numerically demonstrated quantitative rescattering (QRS) theory [11–13] or the three-step analytic formulas for HHG [14–16] have shown that signatures of multielectron effects should be visible in the HHG spectra. The QRS theory [11–13] and the analytical formulation [14–16] both rely on the key idea that there is a close connection between an atom's or molecule's HHG spectrum (via the photorecombination cross section) and its field-free photoionization cross section. These predictions have been confirmed experimentally [17], since the well-known

giant dipole resonance (through interchannel many-electron correlations) in the $4d$-subshell photoionization cross section of Xe was found to strongly influence the HHG spectra. Similarly, the strong resonances evidenced experimentally in HHG spectra of the Cr^+ and Mn^+ transition-metal ions [18,19] were explained theoretically [20] as stemming from well-known intense $3p \rightarrow 3d$ inner-shell transitions in the photoionization cross sections of those ions. Also, the prominent feature near 60 eV observed experimentally in the supercontinuum spectrum of He was attributed to the $2s2p$ ($^1P^o$) autoionizing state [21]. In this tunneling regime, a general feature is that the HHG spectrum exhibits the well-known plateau structure (in which intensities of harmonics remain roughly constant) [7]. This nonperturbative feature stems from rescattering effects of the freed electron, and the cutoff (where generation efficiency drops dramatically) occurs at the odd harmonic order N closest to $E_b + 3.17U_p$ [22].

In the multiphoton regime, several theoretical [23–34] and experimental [23,35–40] works have demonstrated resonance effects or multielectron effects on the HHG spectra of atoms. In particular, effects of the $2s2p$ ($^1P^o$) doubly excited state of He (initially in its ground state) on the HHG spectrum were well evidenced [33]. More interesting, effects of both the $2p4s$ $^1P^o$ and $2p5s$ $^1P^o$ doubly excited states of Be (initially in its ground state) on the HHG spectra were found to lead to an increase by an order of magnitude over a range of harmonics that form a plateau, extending from the resonant harmonic up to a cutoff at the 25th harmonic [34]. However, when each of the resonant harmonics was in resonance with a given autoionizing state, there was also a low-order multiphoton resonance with singly excited states [e.g., the $1snp$ $^1P^o$ singly excited states in He or the $2s2p$ ($^1P^o$) singly excited state in Be]. Thus, whether this multiphoton regime plateau structure is due to either doubly excited state resonances or singly excited state resonances is still puzzling. Finally, whether this plateau feature seen in the HHG spectra of Be also occurs in the HHG spectra of He needs to be elucidated.

In this paper, in order to shed light on the origin of the multiphoton regime plateau structure predicted in the HHG spectra of two-active-electron atoms (e.g., Be [34]),

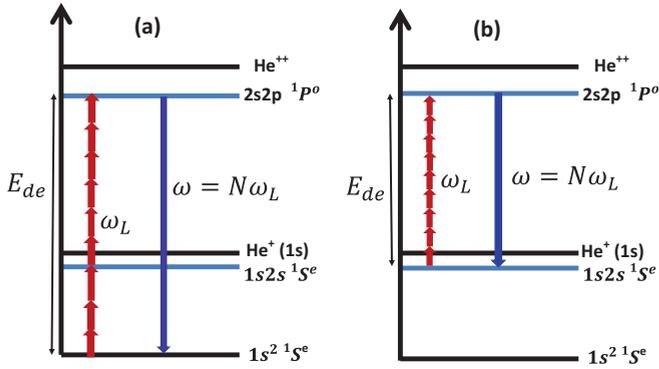*Corresponding author: marcelngoko@unl.edu

†Deceased

FIG. 1. Schematic energy level diagram showing (a) the $1s^2$ ($^1S^e$) ground-state and (b) the $1s2s$ ($^1S^e$) state as an initial state for production of harmonics by a strong laser field with frequency ω_L. The red arrows indicate a nine-photon transition from the corresponding initial state to the He $2s2p$ ($^1P^o$) autoionizing state followed by harmonic emission ($\omega = N\omega_L$) back to the same initial state. The binding energy in (a) is $E_b = 24.6$ eV, while it is $E_b \simeq 4.18$ eV in (b).

we propose to study the sensitivity of the HHG spectra for helium atoms to their initial quantum state. For the helium atom being initially either in its $1s^2$ ($^1S^e$) ground state or in its $1s2s$ ($^1S^e$) excited metastable state that is exposed to an intense linearly polarized flat-top laser field with a resonant driving frequency ω_L^{res} such that $\Omega_q^{res} \equiv q\omega_L^{res}$ is resonant to the transition between the initial state and the $2s2p$ ($^1P^o$) doubly excited state, we solve the full-dimensional two-electron time-dependent Schrödinger equation (TDSE) and calculate the HHG spectra. The rationale behind this strategy is that when starting from an excited state (rather than the ground state as in Refs. [33,34]), singly excited state resonances can be excluded from analyses for production of HHG plateau. Thus, any plateau feature in the HHG spectra would be exclusively due to doubly excited state resonances.

Focusing on the resonant $q = 9$ harmonic, our findings are threefold. First, the intensity of the resonant ninth harmonic in the HHG spectra obtained from these two initial states is found to be significantly enhanced relative to its direct neighbors. Second, when He atom is initially in its $1s^2$ ($^1S^e$) ground state [as illustrated in Fig. 1(a)] we find that a plateau structure is formed from the resonant ninth harmonic and extends up to the 25th harmonic, while when He atom is initially in the $1s2s$ ($^1S^e$) singly excited state [as illustrated in Fig. 1(b)] there is no such a plateau structure. Third, by varying the laser driving frequency ω_L near the resonant driving frequency ω_L^{res} for the initial $1s2s$ ($^1S^e$) singly excited state, an asymmetric Fano-like resonance profile [with a width $\Gamma_{2s2p} \simeq 0.037$ eV equals that for the $2s2p$ ($^1P^o$) autoionizing state] is directly observed in the energy-integrated harmonic power $A_9(\omega_L)$ for the resonant ninth harmonic. However, this observation occurs for a laser peak intensity in the range 7–15 TW/cm^2. This latter result contrasts with that obtained for the initial ground state since the spectroscopic observable that exhibits the same feature is not $A_9(\omega_L)$, but instead the ratio $A_9(\omega_L)/A_7(\omega_L)$ between the resonant ninth harmonic and the nonresonant seventh harmonic. Indeed, when the ninth harmonic is tuned on resonance

with the nine-photon transition between the ground state and the $2s2p$ ($^1P^o$) doubly excited state, there is a three-photon resonance between the ground state and the intermediate $1s2p$ ($^1P^o$) singly excited state. Thus, not only the third harmonic is largely enhanced, but also the higher-order harmonics (including the seventh and the ninth harmonics). Therefore, taking the ratio $A_9(\omega_L)/A_7(\omega_L)$ eliminates the contribution for the intermediate $1s2p$ ($^1P^o$) singly excited state and isolates the contribution for the $2s2p$ ($^1P^o$) doubly excited state. We note that the evidence of doubly excited states on HHG spectra only occurs for a driving laser with duration longer than the lifetime of these autoionizing states [32–34]. All these results show that the plateau structure observed in the HHG spectra produced in the multiphoton regime originates mostly from singly excited state resonances.

This paper is organized as followed. In Sec. II, we briefly describe our numerical method in obtaining the dipole velocity from which the HHG spectrum is calculated. In Sec. III, we present our numerical HHG results for the two initial-state schemes illustrated in Fig. 1(a) and Fig. 1(b). In Sec. IV, we summarize our results and draw some conclusions. Atomic units (a.u.) are used throughout this paper unless specified otherwise.

II. NUMERICAL METHOD

The *ab initio* calculation of the HHG spectrum for the He atom being initially in its ground or singly excited state is obtained as in Refs. [32–34], i.e., using the wave packet solution of the two-electron TDSE. Our numerical methods are presented in detail in Sec. II B of Ref. [33]. Thus, in the following only a summary of key points is provided. The laser-atom interaction is treated within the electric dipole approximation. Owing to gauge invariance, the HHG spectrum can in principle be evaluated using the induced dipole in the length, velocity, or acceleration gauge. However, use of either the length gauge or the acceleration gauge requires accurate two-electron wave packets at either large or small radial coordinates, respectively, whereas the velocity gauge requires accurate wave packets at intermediate radial coordinates. We employ a moderate laser peak intensity of 7–130 TW/cm^2. Despite the small binding energy for the $1s2s$ ($^1S^e$) excited state ($E_b \simeq 4.18$ eV), we carry out our calculations for driving laser frequencies in the range within which lies the fundamental of the tunable KrF laser, that is also comparable to the frequency range used in Ref. [33] where the He atom was initially in its ground state. With these choices of laser parameters, we are always in the multiphoton regime where the ponderomotive energy and the quiver amplitude never exceed 0.08 eV and 0.86 a.u., respectively. We find that calculating the induced dipole in the velocity gauge within a radial box of $r_0 = 30$ a.u. gives converged results for the HHG spectrum of He.

The full-dimensional two-electron TDSE describing the interaction of He with a laser field in the electric dipole approximation and the velocity gauge reads:

$$i\partial_t \Psi_v(\mathbf{r}_1, \mathbf{r}_2, t) = [H_0 + \mathbf{A}(t) \cdot (\mathbf{p}_1 + \mathbf{p}_2)]\Psi_v(\mathbf{r}_1, \mathbf{r}_2, t), \quad (1)$$

where the nonrelativistic field-free Hamiltonian H_0 is

$$H_0 = \frac{p_1^2}{2} + \frac{p_2^2}{2} - \frac{2}{r_1} - \frac{2}{r_2} + \frac{1}{|\mathbf{r}_1 - \mathbf{r}_2|}, \qquad (2)$$

with $\mathbf{r}_1, \mathbf{r}_2$ and $\mathbf{p}_1, \mathbf{p}_2$ being, respectively, the spatial and momentum coordinates of the two electrons. In Eq. (1), the vector potential and the electric field linearly polarized along the z axis are defined in the time interval $-T/2 \leqslant t \leqslant T/2$ as:

$$\mathbf{A}(t) = A_0 f(t) \sin(\omega_L t + \phi)\mathbf{e}_z, \quad \mathbf{E}(t) = -\partial_t \mathbf{A}(t), \qquad (3)$$

where ω_L is the frequency of the driving laser, ϕ is its carrier-envelope phase (CEP), and T is its total duration. The laser peak intensity is given by $I = E_0^2$, where $E_0 = A_0 \omega_L$ is the laser amplitude. Toma *et al.* [23] have found experimentally that resonance effects in HHG that may not be visible for a Gaussian-shaped focus, could be observed for a spatially shaped flat top focus. Hence, here the pulse envelope, $f(t)$, in our calculations has a trapezoidal (flat-top) profile, where the laser pulse is ramped on and off over eight optical cycles, with a total duration of $N_c = 30$ optical cycles. Owing to this large number of optical cycles, CEP effects are negligible.

The flexibility of our numerical method used here and in Refs. [33,34] allows us to prepare an arbitrary field-free initial state from which its evolution [see Eq. (1)] in the presence of the laser field can be solved accurately using an embedded Runge-Kutta method of order 5. Note that for both initial states and laser parameters considered here, the norm of the wave packet is always well conserved. Once the time-dependent wave functions $\Psi_v(\mathbf{r}_1, \mathbf{r}_2, t)$ are obtained, the expectation value of the dipole velocity operator $d_v(t)$ is calculated as in [33,34]:

$$d_v(t) = \langle \Psi_v(\mathbf{r}_1, \mathbf{r}_2, t)|\pi_{z_1} + \pi_{z_2}|\Psi_v(\mathbf{r}_1, \mathbf{r}_2, t)\rangle, \qquad (4)$$

where $\pi_{z_1} = p_{z_1} - A$ and $\pi_{z_2} = p_{z_2} - A$ define the kinematical momenta, which differ from the canonical momenta p_{z_1} and p_{z_2} by the vector potential. The power $\mathcal{P}(\omega_L; \omega)$ of the harmonic radiation with frequency ω induced by the laser field is

$$\mathcal{P}(\omega_L; \omega) = |d(\omega)|^2, \quad d(\omega) = \frac{i}{\omega T} \int_{-T/2}^{T/2} dt \, e^{-i\omega t} d_v(t). \quad (5)$$

We employ ten values of the total angular momentum L, where $0 \leqslant L \leqslant 9$ [34]. For each total angular momentum L, we use four pairs of individual electron angular momenta (l, l'), i.e., for a given L and a given value of l, where $0 \leqslant l \leqslant 6$, we chose l' according to the usual angular momentum and parity selection rules and, to avoid redundancy, $l \leqslant l'$.

III. NUMERICAL RESULTS

In this part, we discuss in Sec. III A the initial-state sensitivity of the HHG spectra of He for a fixed laser driving frequency and intensity, including electron correlation effects. Section III B is devoted to the dependence of the HHG spectra on the driving frequency. Finally, the variation of the energy-integrated harmonic power for the resonant ninth harmonic as a function of the driving frequency is discussed in Sec. III C.
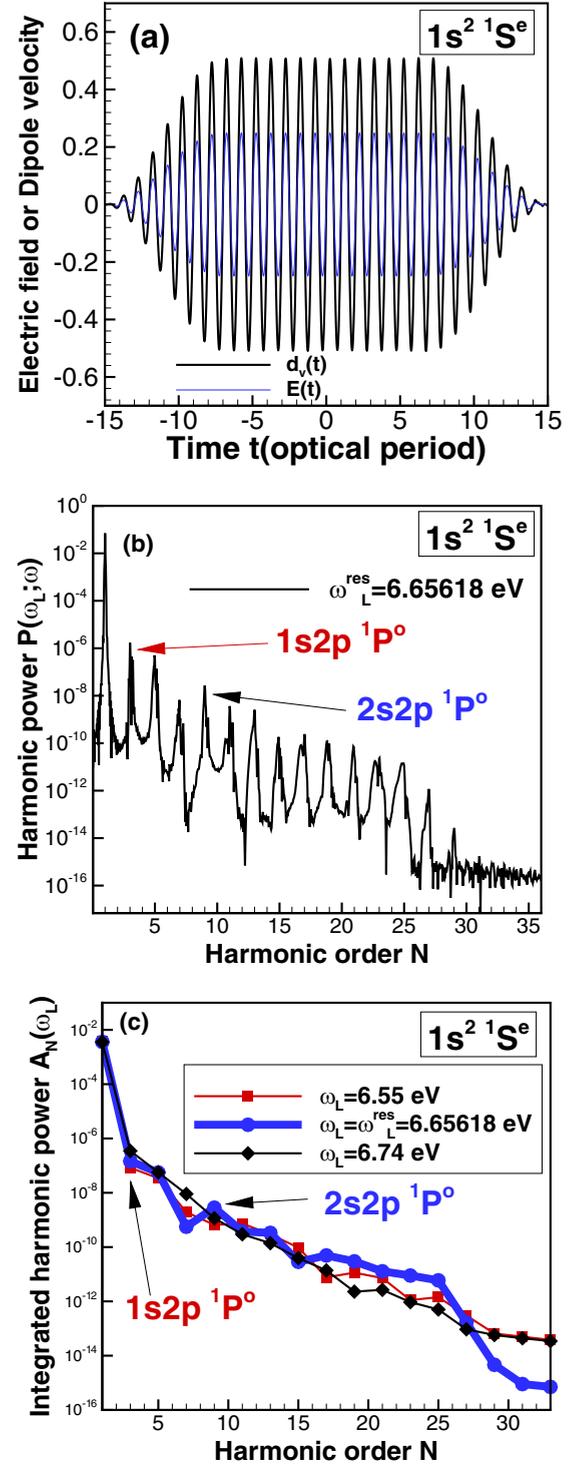

FIG. 2. (a) Time dependence of the scaled electric field [see Eq. (3)] and the induced dipole velocity [see Eq. (4)] for a 30-cycle flat-top laser field at the resonant frequency $\omega_L = \omega_L^{res} \equiv E_{de}/9 = 6.65618$ eV, where E_{de} is the energy gap between the initial $1s^2$ ($^1S^e$) ground state and the $2s2p$ ($^1P^o$) doubly excited state. (b) The TDSE results for the harmonic spectrum [see Eq. (5)]. The pulse intensity is $I = 1.3 \times 10^{14}$ W/cm^2, corresponding to a Keldysh parameter of $\gamma = 5.3$; i.e., the multiphoton regime prevails. (c) Integrated harmonic power $A_N(\omega_L)$ [see Eq. (6)] for three driving frequencies: $\omega_L = 6.55$ eV (off-resonance), $\omega_L = \omega_L^{res}$ (on-resonance), and $\omega_L = 6.74$ eV (off-resonance).

A. Initial-state sensitivity of the HHG spectra

In order to analyze the dependence of the HHG spectrum (5) on the target initial state, we consider the two cases defined in Figs. 1(a) and 1(b). In Fig. 1(a), the helium atom is initially in its $1s^2$ ($^1S^e$) ground state with an energy $E_i = 0$, and its binding energy is $E_b = 24.59$ eV; while in Fig. 1(b), it is initially in the $1s2s$ ($^1S^e$) excited state with an energy $E_i = 20.41$ eV above the ground state, and its binding energy for the $2s$ electron is $E_b \simeq 4.18$ eV. To couple by nine-photon transition each of these initial states with the $2s2p$ ($^1P^o$) doubly excited state (having an energy $E_{2s2p} \simeq 59.9$ eV above the ground state), we use a driving frequency $\omega_L^{res}(1s^2) \equiv (E_{2s2p} - E_i)/9 \simeq 6.65618$ eV for He initially in its ground state, and $\omega_L^{res}(1s2s) \simeq 4.388$ eV for He initially in the $1s2s$ ($^1S^e$) singly excited state. The corresponding scaled electric field $E(t)$ [Eq. (3)] for our flat-top laser field is shown by solid thin blue curves in Fig. 2(a) for $\omega_L = \omega_L^{res}(1s^2)$ and intensity $I = 130$ TW/cm^2 or in Fig. 3(a) for $\omega_L = \omega_L^{res}(1s2s)$ and intensity $I = 10$ TW/cm^2. These pulse intensities in Figs. 2 and 3 are chosen such that they correspond to the same value of the Keldysh parameter, $\gamma = \sqrt{E_b/2U_p} = 5.3$, where $U_p = I/(4\omega_L^2)$ is the ponderomotive energy. Shown in solid thick black curve in Fig. 2(a) or in Fig. 3(a), is the corresponding time-dependent expectation value for the dipole velocity $d_v(t)$ [Eq. (4)]. One sees that the dipole velocity $d_v(t)$ [Eq. (4)] oscillates with a period $2\pi/\omega_L^{res}$ of 0.62 fs for the initial ground state and of 0.94 fs for the $1s2s$ ($^1S^e$) singly excited state, but it is always in phase with the electric field. However, the shape of $d_v(t)$ differs dramatically whether He is initially in its ground state or in that excited state. In the former case, the shape of $d_v(t)$ mimics that of the electric field. In the latter case, $d_v(t)$ while oscillating with the laser field, undergoes a large single oscillation around the flat-top part of the laser field for $-9T_0 \leqslant t \leqslant +9T_0$.

As the laser field may deplete the initial state by populating excited states and continuum states, it is legitimate to wonder whether this difference in the temporal shape of the dipole velocity is due to ionization or excitation? In Fig. 1(a) single ionization of the He ground state ($E_b \simeq 24.6$ eV) at the resonant photon energy $\omega_L^{res}(1s^2) \equiv 6.65618$ eV requires at least four photons to occur, while in Fig. 1(b) single ionization of the $1s2s$ ($^1S^e$) excited state at the resonant photon energy $\omega_L^{res}(1s2s) \equiv 4.388$ eV (greater than $E_b = 4.18$ eV) is already possible by single-photon absorption. For the pulse parameters specified above for which $\gamma = 5.3$ for the two schemes in Figs. 1(a) and 1(b), our TDSE results for the temporal behavior of the initial-state populations are shown in Fig. 4(a) for the ground state and in Fig. 4(b) for the $1s2s$ ($^1S^e$) excited state. The probability for combined ionization and excitation extracted from those populations at the end of the laser pulse gives 0.06% for the scheme in Fig. 1(a) and 3.3% for the scheme in Fig. 1(b). Moreover, the calculated amount of ionization for the initial ground state is very weak (0.04%), while it is larger (1.5%) but still small for the initial $1s2s$ ($^1S^e$) excited state. We note that significant ionization in the scheme Fig. 1(b) would lead to an irreversible loss of population of bound states, and consequently, would lead to a monotonic decrease in the dipole velocity with time. However, one sees in Fig. 3(a) that the decay of the dipole velocity with time
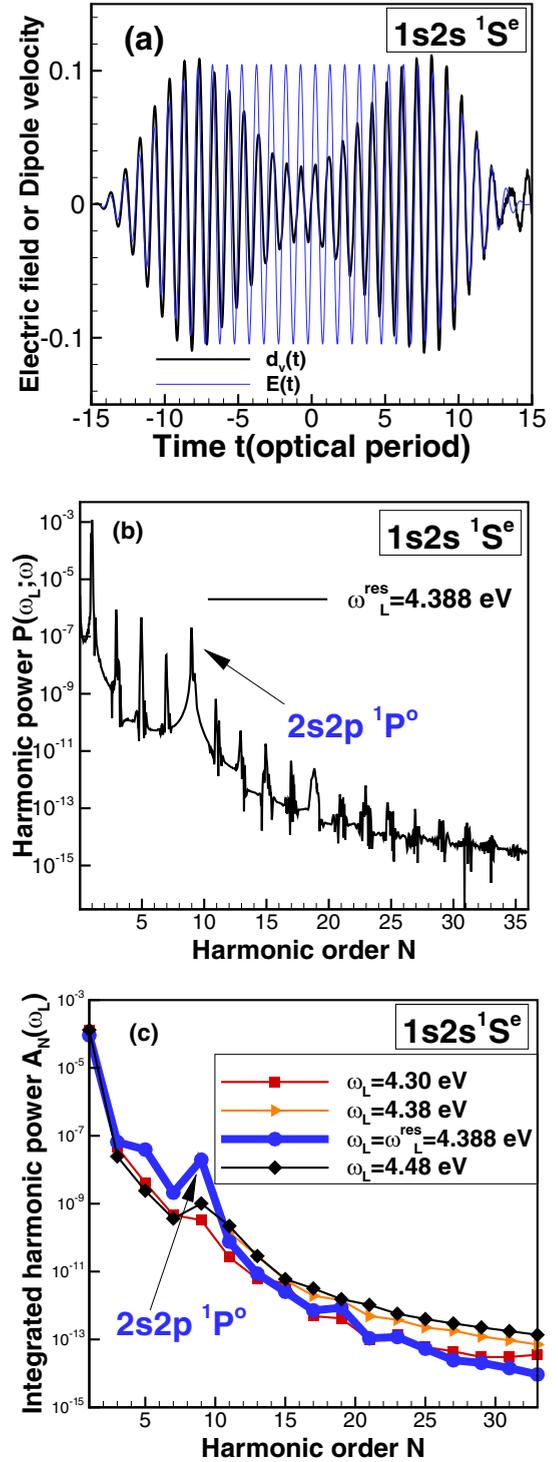

FIG. 3. Same as in Fig. 2 but for the case where the He atom is initially in the $1s2s$ ($^1S^e$) excited state, which is located at $E_{de} \simeq 39.49$ eV below the $2s2p$ ($^1P^o$) doubly excited state and about 20.41 eV above the ground state. The corresponding resonant driving frequency for the ninth harmonic is $\omega_L^{res} \equiv E_{de}/9 = 4.388$ eV. The two driving frequencies for off-resonance cases used in (c) for comparison are $\omega_L = 4.30$ eV and $\omega_L = 4.48$ eV. The pulse intensity is set to 10^{13} W/cm^2 in order to keep the same Keldysh parameter $\gamma = 5.3$ used in Fig. 2.
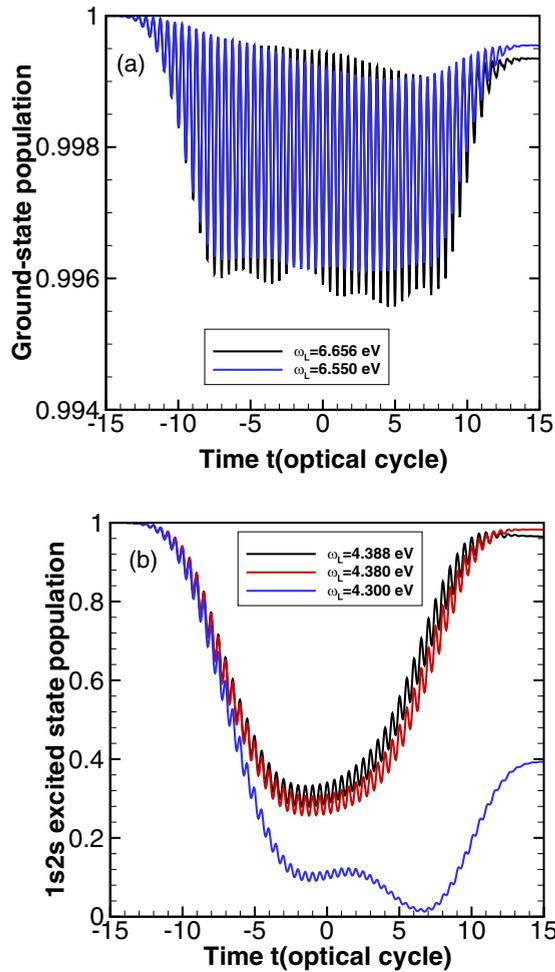
FIG. 4. Time-dependent populations for (a) the initial ground state at the driving frequencies $\omega_L = \omega_L^{\text{res}} = 6.656$ eV and $\omega_L = 6.55$ eV; and (b) the initial $1s2s$ ($^1S^e$) excited state at the driving frequencies $\omega_L = \omega_L^{\text{res}} = 4.388$ eV, $\omega_L = 4.380$ eV, and $\omega_L = 4.300$ eV. The pulse parameters in (a) and (b) are the same in Fig. 2 and Fig. 3, respectively.

changes to its growth, which cannot be due to a dissipative dynamics. We thus deduce that this time-dependent effect in the dipole velocity can only be due to excitation of bound states; there is a beating of populations between the initial and final bound states.

Analyses of the time-dependent populations in Fig. 4 show that, while oscillating with the laser field, there is a small amount of single excitation and double excitation in the scheme Fig. 1(a) with a maximum of ~0.4% and a large amount of double excitation in the scheme Fig. 1(b) with a maximum of ~70%. For the scheme in Fig. 1(a), as the ground state is nearly not depleted [see Fig. 4(a)] this excitation dynamics is well reflected in the dipole velocity shown in Fig. 2(a), which simply mimics the laser field shape. For the scheme in Fig. 1(b), the period of about $18T_0 \approx 17$ fs of the large oscillation exhibited by the dipole velocity in Fig. 3(a) or by the population in Fig. 4(b) is close to 17.7 fs, the lifetime of the $2s2p$ ($^1P^o$) doubly excited state. We note that Hu and Collins [41] used a 100-cycle (10.7 fs) sine-squared pulse with a photon energy of 38.8 eV and an intensity of 60 TW/cm^2

to resonantly excite the $2s2p$ ($^1P^o$) doubly excited state in the scheme Fig. 1(b) with a probability over 80%. After the laser pulse dies off, the decay dynamics of autoionization for the $2s2p$ ($^1P^o$) doubly excited state was observed when letting the two-electron system freely evolve in time for another 200 cycles (21.4 fs). Here, Fig. 4(b) shows that about 12 cycles (11 fs) is needed to resonantly drive 70% of population of the initial $1s2s$ ($^1S^e$) state into the $2s2p$ ($^1P^o$) doubly excited state, which corresponds to the decay in the dipole velocity with time seen in Fig. 3(a). The change to its growth for times $t > 0$ of the dipole velocity in Fig. 3(a) or of the population in Fig. 4(b) reflects the process of double deexcitation of the $2s2p$ ($^1P^o$) doubly excited state into the initial $1s2s$ ($^1S^e$) state, together with ongoing laser-assisted autoionization of the $2s2p$ ($^1P^o$) state.

The calculated HHG spectra [see Eq. (5)] for these two initial states are displayed in Fig. 2(b) and in Fig. 3(b), respectively. They are obtained by taking the Fourier transform of the dipole velocity $d_v(t)$ [see Eq. (4)] given in Figs. 2(a) and 3(a). Effects of the $2s2p$ ($^1P^o$) autoionizing state on the HHG spectrum in each case are striking. In Figs. 2(b) and 3(b), one sees that the intensity of the resonant ninth harmonic is higher than that for its direct neighbors, namely, the seventh and eleventh harmonics. Moreover, in Fig. 2(b) harmonics beyond the resonant ninth harmonic have roughly the same intensity; they thus form a plateau structure with a cutoff located at the 25th harmonic, just as in Ref. [34] for the Be atom. Furthermore, in Fig. 3(b) one sees that the intensities of harmonics beyond the resonant ninth harmonic are perturbatively decreasing and no plateau structure occurs.

The harmonics produced in Fig. 2(b) and Fig. 3(b) are not monochromatic. In order to account for such nonmonochromaticity of harmonics, it is thus useful to introduce the physical quantity, $A_N(\omega_L)$, defined as the harmonic power integrated over the energies from $(N-1)\omega_L$ to $(N+1)\omega_L$, at each harmonic order N [33,34]:

$$A_N(\omega_L) = \int_{(N-1)\omega_L}^{(N+1)\omega_L} \mathcal{P}(\omega_L; \omega) d\omega. \tag{6}$$

The HHG spectrum for $A_N(\omega_L)$ (6) when He is initially in the ground state or in the $1s2s$ ($^1S^e$) excited state is shown in Fig. 2(c) or in Fig. 3(c), respectively. Analyses of the two energy-integrated harmonic spectra confirm the observations based on the intensity of harmonics, namely, a multiphoton-regime plateau structure does occur in the HHG spectra for the initial ground state, and does not occur for the initial $1s2s$ ($^1S^e$) excited state.

B. Driving frequency sensitivity of the HHG spectra of He

The presence or absence of plateau depending upon the initial quantum state is quite intriguing, but what is the origin of this plateau structure. We note that only the $2s2p$ ($^1P^o$) doubly excited state is involved when producing harmonics from the initial $1s2s$ ($^1S^e$) excited state, while the $2s2p$ ($^1P^o$) doubly excited state as well as singly excited states can be involved when HHG are produced from the initial He ground state. To see this, we study here the sensitivity of the whole HHG spectra to the driving frequency for a given initial quantum state.

For the case of He being initially in its ground state, three driving frequencies are considered in Fig. 2(c). These include the resonant frequency $\omega_L = \omega_L^{\text{res}}(1s^2) \simeq 6.65618$ eV, and the two off-resonance frequencies $\omega_L = 6.55$ eV and 6.74 eV. The time-dependent ground-state populations for the resonant case and the nonresonant case ($\omega_L = 6.55$ eV) are compared in Fig. 4(a). One sees that the temporal behaviors of these two populations only differ slightly in their shapes, which is mainly due to correlated resonance effects. Figure 2(c) shows that the energy-integrated HHG spectra for both on-resonance and off-resonance cases exhibit a multiphoton regime plateau structure, however, the drop in harmonic efficiency from the cutoff position at the 25th harmonic is sharper in the resonant case. For these three driving frequencies, $\Omega_3 \equiv 3\omega_L$ are, respectively, ~ 20 eV, 19.65 eV, and 20.22 eV; which are just about 1 eV below the He $1s2p$ $(^1P^o)$ singly excited state (located at 21.0 eV above the ground state). In other words, the intermediate $1s2p$ $(^1P^o)$ singly excited state becomes significantly more populated by three-photon transition from the ground state when the driving frequency ω_L increases from 6.55–6.74 eV.

For the case of He being initially in the $1s2s$ $(^1S^e)$ singly excited state, four driving frequencies are considered in Fig. 3(c), namely, $\omega_L = 4.30$ eV and 4.48 eV for off-resonance cases, $\omega_L = 4.380$ eV for the slightly on-resonance case, and $\omega_L = \omega_L^{\text{res}} = 4.388$ eV for the on-resonance case. One sees in Fig. 3(c) that the harmonic spectra for $\omega_L = 4.30$ eV and 4.48 eV are nearly the same below the ninth harmonic. However, they differ from each other for the ninth harmonic and above, with the harmonic spectrum for $\omega_L = 4.48$ eV being always higher than that for $\omega_L = 4.30$ eV. The little enhancement observed in Fig. 3(c) for the ninth harmonic at these two nearly off-resonance frequencies are due to the rather small values (0.088 eV and 0.092 eV) for the detuning $\Delta \equiv \omega_L - \omega_L^{\text{res}}$ in each case. We note that the ionization probability at $\omega_L = 4.30$ eV is 45%, while it is 23% at $\omega_L = 4.48$ eV. Also, the time dependence of the initial-state population for these two nonresonant cases [see e.g., Fig. 4(b) for $\omega_L = 4.30$ eV] evidences the fact that the process of HHG occurs with significant ionization. This is in contrast to the resonant case where the amount of ionization is less than 2%.

At the resonant frequency $\omega_L = \omega_L^{\text{res}} = 4.388$ eV and the slightly on-resonance frequency $\omega_L = 4.380$ eV, Fig. 3(c) shows that the two harmonic spectra coincide up to the 11th harmonic, with a dramatic enhancement for the resonant ninth harmonic. However, beyond the 11th harmonic the two harmonic spectra decrease monotonically with the energy-integrated harmonic power being larger for $\omega_L = 4.38$ eV than for $\omega_L = \omega_L^{\text{res}} = 4.388$ eV. The time dependence of the initial-state populations for these resonant and slightly resonant cases shown in Fig. 4(b) exhibit only some small but noticeable differences for $t > 0$. These small differences are responsible for the difference in the harmonic intensity seen in Fig. 3(c) beyond the 11th harmonic. We note that for $t > 0$, the process of deexcitation is accompanied with modifying autoionization decay produced the laser field.

The present work and previous works [32–34] have found that effects of doubly excited states on the HHG spectra (regardless of the initial quantum state) are only visible for a total pulse duration, T, longer than the lifetime, τ, of

autoionizing states. Here, the total duration of the laser field is $T \simeq 28$ fs, which is longer than the lifetime, $\tau = 17.7$ fs, of the $2s2p$ $(^1P^o)$ autoionizing state; meaning that autoionization in the presence of the laser field is taking place. Besides the rather comparable amount of direct ionization at these two frequencies, autoionization is more significant for $\omega_L = \omega_L^{\text{res}} = 4.388$ eV than for $\omega_L = 4.38$ eV since the calculated amount of ionization for the laser duration used is 1.5% at $\omega_L = \omega_L^{\text{res}} = 4.388$ eV and 0.8% at $\omega_L = 4.38$ eV. This small leak via autoionization is at the expense of harmonic generation. In particular, the interaction of the ninth harmonic [that is close on resonance with or is resonant with the transition between the initial state and the $2s2p$ $(^1P^o)$ doubly excited state] with higher-order harmonics is weakened by ongoing laser-assisted autoionization so that it cannot support a plateau structure at the laser intensity used.

For the laser parameters used here, the fact that a plateau structure is absent in the HHG spectrum when only doubly excited states are involved and is present when both singly excited states and doubly excited states are involved demonstrates that the multiphoton-regime plateau structure formed in the HHG spectrum for the ground state of helium (and beryllium [34]) stems mainly from the intermediate singly excited state populated by low-order transition. These atomic resonances as origin of this multiphoton regime HHG plateau clearly differ from that of the strong-field low-frequency tunneling regime HHG plateau, which originates from rescattering effects of the freed electron.

C. Driving frequency sensitivity of the resonant ninth harmonic

It is important that our above analysis is based on the field-free energies for the He atom. However, in the presence of a strong laser field, it is well known that the excitation energies of the singly and doubly excited states may be shifted. Thus, in order to resolve the actual position of the $2s2p$ $(^1P^o)$ doubly excited state in presence of the employed strong laser field, below we present a study for the energy-integrated harmonic power when varying the driving frequency ω_L near the field-free resonant frequency ω_L^{res}. The goal here is to show how the process of HHG can be viewed as a powerful spectroscopy tool.

For the initial He ground state, we show in Fig. 5(a) the dependence to the driving frequency ω_L of the energy-integrated harmonic powers $A_9(\omega_L)$ and $A_7(\omega_L)$, for, respectively, the resonant ninth harmonic and the nonresonant seventh harmonic. Here, we scan the driving frequency ω_L over a small energy range 6.55–6.74 eV across the field-free resonant frequency $\omega_L^{\text{res}}(1s^2) \simeq 6.65618$ eV. One sees that $A_9(\omega_L)$ exhibits a broad resonance, with a peak located at $\omega_L = \omega_L^{\text{res}}$, and a width that is twice that of the $2s2p$ $(^1P^o)$ autoionizing state. In the meantime, one observes that $A_7(\omega_L)$ undergoes an oscillation: it increases for $\omega_L < 6.61$ eV and reaches its maximum at $\omega_L = 6.61$ eV; it then decreases for 6.61 eV $\leqslant \omega_L \leqslant \omega_L^{\text{res}}$ while crossing $A_9(\omega_L)$ at $\omega_L \simeq 6.63$ eV; next, it saturates for $\omega_L^{\text{res}} \leqslant \omega_L \leqslant 6.68$ eV; and finally increases for $\omega_L > 6.68$ eV while crossing $A_9(\omega_L)$ a second time at $\omega_L \simeq 6.695$ eV. This oscillatory shape for $A_7(\omega_L)$ and broad resonance for $A_9(\omega_L)$ indicate a strong coupling between the seventh and ninth
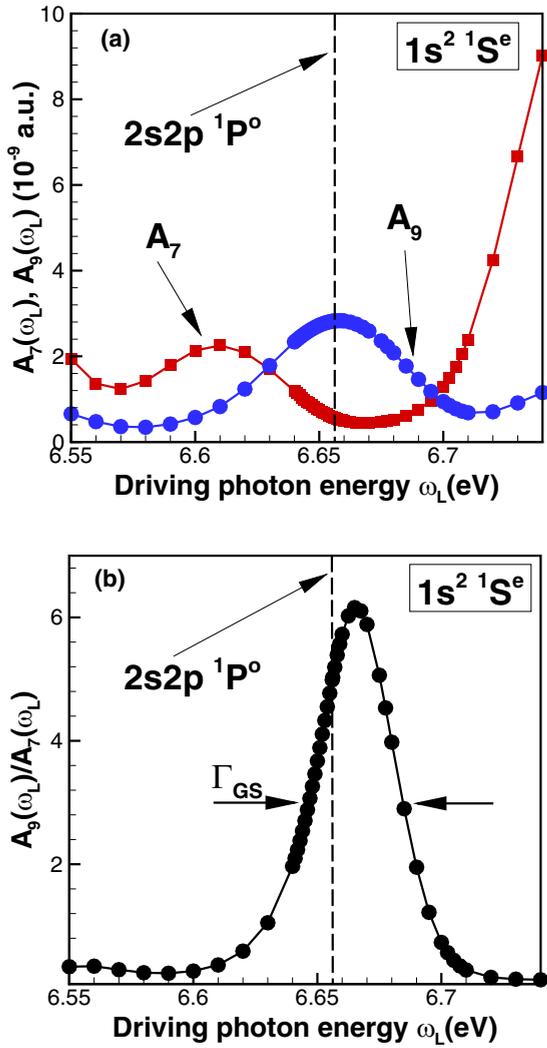
FIG. 5. Initial ground state: (a) Variation with the driving frequency ω_L (near the resonant frequency $\omega_L^{\text{res}} \equiv 6.65618$ eV) of the integrated harmonic power $A_7(\omega_L)$ and $A_9(\omega_L)$ for the nonresonant seventh harmonic and the resonant ninth harmonic. (b) The corresponding variation of the ratio $A_9(\omega_L)/A_7(\omega_L)$ with the driving frequency ω_L. The vertical bar marks $\omega_L = \omega_L^{\text{res}}$, at which the ninth harmonic is resonant with the transition from the initial $1s^2$ ($^1S^e$) ground state to the $2s2p$ ($^1P^o$) doubly excited state. The other laser parameters are specified in the caption of Fig. 2. In (b) the ratio $A_9(\omega_L)/A_7(\omega_L)$ exhibits a Fano resonance profile with a width $\Gamma_{\text{GS}} \simeq 0.037$ eV, while in (a) the integrated resonant-harmonic power $A_9(\omega_L)$ exhibits a broader resonance.

FIG. 6. Initial excited state: (a) Variation with the driving frequency ω_L (near the resonant frequency $\omega_L^{\text{res}} \equiv 4.388$ eV) of the integrated harmonic power $A_7(\omega_L)$ and $A_9(\omega_L)$ for the nonresonant seventh harmonic and the resonant ninth harmonic. (b) The corresponding variation of the ratio $A_9(\omega_L)/A_7(\omega_L)$ with the driving frequency ω_L. The vertical bar marks $\omega_L = \omega_L^{\text{res}}$, at which the ninth harmonic is resonant with the transition from the initial $1s2s$ ($^1S^e$) excited state to the $2s2p$ ($^1P^o$) doubly excited state. The other laser parameters are specified in the caption of Fig. 3. In contrast to Fig. 5(a), the corresponding integrated resonant-harmonic power $A_9(\omega_L)$ in (a) exhibits a Fano resonance profile with a width $\Gamma_{\text{ES}} \simeq 0.034$ eV.

harmonics mediated by the $2s2p$ ($^1P^o$) doubly excited state resonance, as can be explained below.

As ω_L covers the range 6.55–6.74 eV, the third harmonic is increasingly tuned on resonance with the $1s2p$ ($^1P^o$) singly excited state (located at 21 eV above the He ground state), since $\Omega_3 = 3\omega_L$ is in the range 19.65–20.22 eV. Thus, all harmonics with order $N > 3$ are coupled with the third harmonic; they are significantly enhanced such that a plateau structure is formed. Although all the harmonics with order $N > 3$ are enhanced, the perturbative expectation that $A_7(\omega_L)$ be larger than $A_9(\omega_L)$ is preserved, as shown by Fig. 5(a) for
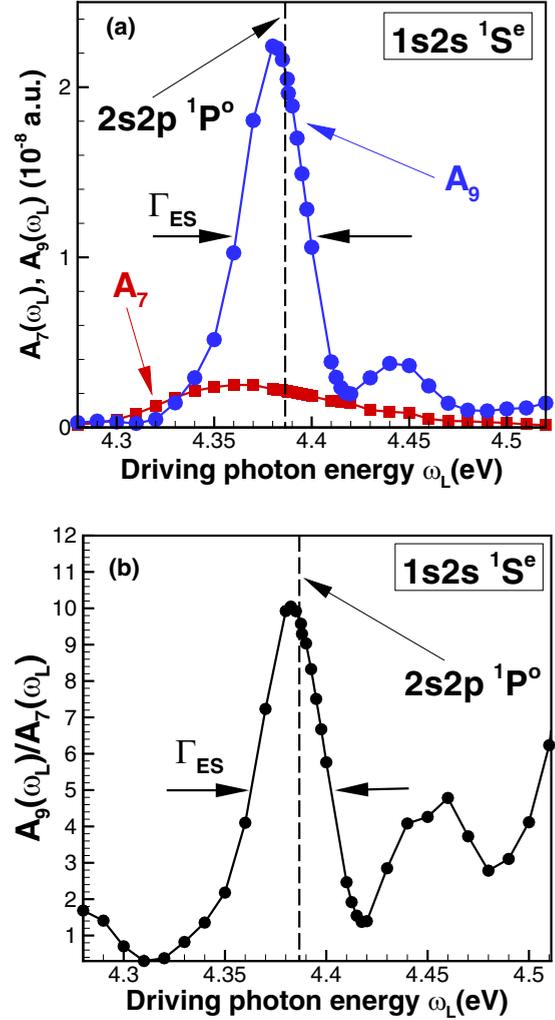
$\omega_L < 6.61$ eV or $\omega_L \geqslant 6.70$ eV (which are off the range over which the $2s2p$ ($^1P^o$) doubly excited resonance influences). However, near the resonant frequency (i.e., for 6.61 eV $\leqslant \omega_L \leqslant 6.70$ eV) the effect of the $2s2p$ ($^1P^o$) doubly excited resonance is to induce a strong interaction between the seventh and the ninth harmonics. Here, one sees that the nonresonant seventh harmonic feeds the resonant ninth harmonic since $A_7(\omega_L)$ presents a concave up pattern, while $A_9(\omega_L)$ exhibits a concave down pattern.

In order to isolate effects of the $2s2p$ ($^1P^o$) doubly excited state on $A_9(\omega_L)$, one must eliminate the global effects of the $1s2p$ ($^1P^o$) singly excited state. As in Refs. [33,34], a suitable

way to achieve this goal is taking the ratio $A_9(\omega_L)/A_7(\omega_L)$ since both the seventh and ninth harmonics are strongly coupled to the third harmonic, which is on resonance with the three-photon transition between the ground state and the $1s2p$ ($^1P^o$) singly excited state. Using the results for $A_7(\omega_L)$ and $A_9(\omega_L)$ in Fig. 5(a), the corresponding ratio $A_9(\omega_L)/A_7(\omega_L)$ shown in Fig. 5(b) exhibits a Fano resonance profile, peaking at $\omega_L = 6.665$ eV (i.e., blue shifted to the field-free position $\omega_L^{\rm res} = 6.65618$ eV by 0.0088 eV), and having a width $\Gamma_{\rm GS} = 0.037$ eV that matches exactly the width of the $2s2p$ ($^1P^o$) autoionizing state.

For the initial $1s2s$ ($^1S^e$) singly excited state, we show in Fig. 6(a) the variation of the energy-integrated harmonic powers $A_9(\omega_L)$ and $A_7(\omega_L)$ as a function of the driving frequency ω_L. Here, we scan the driving frequency ω_L over a small energy range 4.28–4.52 eV across the field-free resonant frequency $\omega_L^{\rm res}(1s2s) = 4.388$ eV. In contrast to Fig. 5(a), which is for the initial ground state, $A_7(\omega_L)$ shown in Fig. 6(a) does not oscillate and is quite always smaller than $A_9(\omega_L)$. Moreover, one sees that $A_9(\omega_L)$ directly exhibits an asymmetric Fano resonance profile with a maximum located at $\omega_L = 4.38$ eV that is very close to the field-free resonant frequency $\omega_L^{\rm res} = 4.388$ eV. Its width is $\Gamma_{\rm ES} \simeq 0.034$ eV, which compares well with the width of 0.037 eV for the $2s2p$ ($^1P^o$) autoionizing state. A virtue of starting from the initial $1s2s$ ($^1S^e$) excited state is that effects of doubly excited states (or electron correlation) can be directly visualized on the energy-integrated harmonic power, $A_9(\omega_L)$, for the resonant ninth harmonic. This is in contrast to the case for atomic target being initially in the ground state where effects of doubly excited states (or electron correlation) is observed rather in the ratio of the integrated harmonic powers between the resonant qth harmonic and the $(q-2)$nd harmonic. For the initial $1s2s$ ($^1S^e$) singly excited state, Fig. 6(b) shows the dependence to ω_L of the corresponding ratio $A_9(\omega_L)/A_7(\omega_L)$. Although the ratio $A_9(\omega_L)/A_7(\omega_L)$ exhibits a resonance profile located at $\omega_L^{\rm res} = 4.38$ eV with the same width $\Gamma_{\rm ES} \simeq 0.034$ eV as in Fig. 6(a), the irregularities in structures on the sides of the resonance profile indicates the nonrationale for taking such ratio in this case.

Finally, we study whether transient phenomena as well as unexpected resonant effects may affect the shape of the whole HHG spectra or a particular harmonic when varying the turn-on duration, $T_{\rm on}$, of our trapezoidal laser field. In all cases, we kept the total pulse duration to 30 cycles and fix the turn-off and turn-on durations to be equal. As $T_{\rm on}$ decreases from eight cycles to two cycles, it follows that the duration of the flat-top part of the laser field increases and we thus find that the intensity of harmonics in Fig. 3(b) increases, but the shape of the whole HHG spectrum hardly changes. For illustration, the shape of the resonance in Fig. 6(a) was investigated as $T_{\rm on}$ decreases; it was found to be insensitive to $T_{\rm on}$ near the frequency range of doubly excited state influence. However, outside that frequency range the presence of some modulation appears for $T_{\rm on} = 2$ cycles. All these results show

that transient phenomena are always absent upon variation of $T_{\rm on}$, while unexpected resonant effects may be present for ultrashort $T_{\rm on}$ of the driving laser pulse.

IV. SUMMARY AND CONCLUSIONS

In summary, by solving the full-dimensional two-electron TDSE for laser field parameters in the multiphoton regime, we have studied the sensitivity to the initial quantum state of the harmonic generation spectrum of the helium atom. For particular laser driving frequencies on resonance with the $2s2p$ ($^1P^o$) doubly excited state, we have discussed how the time-dependent dipole velocity, the whole HHG spectra, and particular harmonics are sensitive to the initial quantum state. For both the initial ground state and the initial $1s2s$ ($^1S^e$) singly excited state, effects of the $2s2p$ ($^1P^o$) doubly excited state are found to significantly enhance the resonant ninth harmonic. By tuning the laser driving frequency across the field-free $2s2p$ ($^1P^o$) doubly excited state resonance, we showed that the energy-integrated resonant ninth harmonic power $A_9(\omega_L)$ for the initial excited state is the relevant physical observable for revealing the position, the width and the shape of the $2s2p$ ($^1P^o$) autoionizing state. In contrast, the relevant spectroscopic observable for the initial ground state is the ratio $A_9(\omega_L)/A_7(\omega_L)$ between the energy-integrated harmonic powers for the resonant ninth harmonic and the nonresonant seventh harmonic, which isolate effects of the $2s2p$ ($^1P^o$) autoionizing state by erasing the global effects of intermediate singly excited states.

This initial-state sensitivity study allows us to shed light on the origin of the predicted multiphoton-regime HHG plateau structure (occurring for the initial ground state and not occurring for the initial excited), which differ from that for the rescattering tunneling regime plateau. Originating from atomic resonances, it is found that multiphoton-regime HHG plateau is more likely produced by low-order resonance transition involving singly excited states than by higher-order resonance transition involving doubly excited states. The evidence of the $2s2p$ ($^1P^o$) autoionizing state on the HHG spectrum occurs only for a laser pulse longer than its lifetime, $\tau_{2s2p} = 17.7$ fs. Thus, a plausible reason that may explain this difference in the origin of the multiphoton-regime HHG plateau is that HHG processes involving doubly excited states may be lossy owing to laser-assisted autoionization, in contrast to HHG processes involving singly excited states.

[1] J. Reintjes, C. Y. She, and R. Eckardt, IEEE J. Quantum Electron. **QE-14**, 581 (1978).

[2] J. Bokor, P. H. Bucksbaum, and R. R. Freeman, Opt. Lett. **8**, 217 (1983).

[3] A. H. Kung, Opt. Lett. **8**, 24 (1983).

[4] E. Marinero, C. Rettner, R. Zare, and A. H. Kung, Chem. Phys. Lett. **95**, 486 (1983).

[5] J. Wildenauer, J. Appl. Phys. **62**, 41 (1987).

[6] A. McPherson, G. Gibson, H. Jara, U. Johann, T. S. Luk, I. A. McIntyre, K. Boyer, and C. K. Rhodes, J. Opt. Soc. Am. B **4**, 595 (1987).

[7] M. Ferray, A. L'Huillier, X. F. Li, L. A. Lompré, G. Mainfray, and C. Manus, J. Phys. B **21**, L31 (1988).

[8] K. J. Schafer, B. Yang, L. F. DiMauro, and K. C. Kulander, Phys. Rev. Lett. **70**, 1599 (1993).

[9] P. B. Corkum, Phys. Rev. Lett. **71**, 1994 (1993).

[10] M. Lewenstein, Ph. Balcou, M. Yu. Ivanov, A. L'Huillier, and P. B. Corkum, Phys. Rev. A **49**, 2117 (1994).

[11] T. Morishita, A.-T. Le, Z. Chen, and C. D. Lin, Phys. Rev. Lett. **100**, 013903 (2008).

[12] A.-T. Le, T. Morishita, and C. D. Lin, Phys. Rev. A **78**, 023814 (2008).

[13] A.-T. Le, R. R. Lucchese, S. Tonzani, T. Morishita, and C. D. Lin, Phys. Rev. A **80**, 013401 (2009).

[14] M. V. Frolov, N. L. Manakov, T. S. Sarantseva, and A. F. Starace, J. Phys. B **42**, 035601 (2009).

[15] M. V. Frolov, N. L. Manakov, T. S. Sarantseva, M. Yu. Emelin, M. Yu. Ryabikin, and A. F. Starace, Phys. Rev. Lett. **102**, 243901 (2009).

[16] M. V. Frolov, N. L. Manakov, T. S. Sarantseva, and A. F. Starace, Phys. Rev. A **83**, 043416 (2011).

[17] A. D. Shiner, B. E. Schmidt, C. Trallero-Herrero, H. J. Wörner, S. Patchkovskii, P. B. Corkum, J.-C. Kieffer, F. Légaré, and D. M. Villeneuve, Nature Phys. **7**, 464 (2011).

[18] R. A. Ganeev, L. B. Elouga Bom, J.-C. Kieffer, and T. Ozaki, Phys. Rev. A **75**, 063806 (2007).

[19] R. A. Ganeev, M. Suzuki, M. Baba, and H. Kuroda, Phys. Rev. A **76**, 023805 (2007).

[20] M. V. Frolov, N. L. Manakov, and A. F. Starace, Phys. Rev. A **82**, 023424 (2010).

[21] S. Gilbertson, H. Mashiko, C. Li, E. Moon, and Z. Chang, Appl. Phys. Lett. **93**, 111105 (2008).

[22] J. L. Krause, K. J. Schafer, and K. C. Kulander, Phys. Rev. Lett. **68**, 3535 (1992).

[23] E. S. Toma, P. Antoine, A. de Bohan, and H. G. Muller, J. Phys. B **32**, 5843 (1999).

[24] M. B. Gaarde and K. J. Schafer, Phys. Rev. A **64**, 013820 (2001).

[25] Z. Zeng, R. Li, Y. Cheng, W. Yu, and Z. Xu, Phys. Scr. **66**, 321 (2002).

[26] C. Figueira de Morisson Faria, R. Kopold, W. Becker, and J. M. Rost, Phys. Rev. A **65**, 023404 (2002).

[27] R. Taieb, V. Veniard, J. Wassaf, and A. Maquet, Phys. Rev. A **68**, 033403 (2003).

[28] A. Kulagin and T. Usmanov, Opt. Lett. **34**, 2616 (2009).

[29] V. Strelkov, Phys. Rev. Lett. **104**, 123901 (2010).

[30] D. B. Milosević, Phys. Rev. A **81**, 023802 (2010).

[31] M. Tudorovskaya and M. Lein, Phys. Rev. A **84**, 013430 (2011).

[32] X. Guan, X.-M. Tong, and S.-I. Chu, Phys. Rev. A **73**, 023403 (2006).

[33] J. M. Ngoko Djiokap and A. F. Starace, Phys. Rev. A **84**, 013404 (2011).

[34] J. M. Ngoko Djiokap and A. F. Starace, Phys. Rev. A **88**, 053412 (2013).

[35] R. A. Ganeev, M. Suzuki, T. Ozaki, M. Baba, and H. Kuroda, Opt. Lett. **31**, 1699 (2006).

[36] M. Suzuki, M. Baba, R. Ganeev, H. Kuroda, and T. Ozaki, Opt. Lett. **31**, 3306 (2006).

[37] M. Suzuki, M. Baba, H. Kuroda, R. A. Ganeev, and T. Ozaki, Opt. Express **15**, 1161 (2007).

[38] S. Haessler, V. Strelkov, L. B. E. Bom, M. Khokhlova, O. Gobert, J.-F. Hergott, F. Lepetit, M. Perdrix, T. Ozaki, and P. Salières, New J. Phys. **15**, 013051 (2013).

[39] R. A. Ganeev, T. Witting, C. Hutchison, V. V. Strelkov, F. Frank, M. Castillejo, I. Lopez-Quintas, Z. Abdelrahman, J. W. G. Tisch, and J. P. Marangos, Phys. Rev. A **88**, 033838 (2013).

[40] R. A. Ganeev, M. Suzuki, S. Yoneya, and H. Kuroda, J. Opt. Soc. Am. B **31**, 3105 (2014).

[41] S. X. Hu and L. A. Collins, Phys. Rev. A **71**, 062707 (2005).